Next Energy 7 (2025) 100245

Contents lists available at ScienceDirect

Next Energy

journal homepage: www.sciencedirect.com/journal/next-energy

Research article

Numerical simulation of an HTL-free carbon-based perovskite solar cell with graphitic carbon nitride doped zinc oxide as electron transport layers

Joseph Kariuki[a], Nicholas Rono[b,*], Chinedu Christian Ahia[b], Eric Kibagendi Osoro[a], Edson L. Meyer[b]

[a] Department of Basic Sciences, Tharaka University, P.O Box 193-60215, Marimanti, Kenya
[b] Institute of Technology, University of Fort Hare, Private Bag X1314, Alice 5700, South Africa

ARTICLE INFO

Keywords:
Perovskite solar cell
Photovoltaic components
HTL-free

ABSTRACT

As a result of the advances in technology and the need for energy, an urge to develop a stable, high performance solar cell has initiated various scientific intentions to attain a cheaper and clean energy supply. In this work, a hole transport free (HTL-free) perovskite solar cell (PSC) with an architecture: FTO/ZnO-g-C_3N_4/$CH_3NH_3PbI_3$/carbon was examined. The simulated device was validated with the already fabricated device in the literature. The electron transport layer (ETL) was a blend with ZnO and graphitic carbon nitride, and named GT1, GT3 and GT5 materials in different ratios. The band gap values of the proposed ETL were 3.06, 3.06, 3.10, and 2.97 eV for pure ZnO, GT1, GT3 and GT5 respectively. Simulations were carried out with an aid of a solar cell capacitance simulator (SCAPS-ID) conducted at AM 1.5 G and 100 mW cm^{-2}. The optimal density defect of the absorber was maintained at 1.0 × 10^{12} cm^{-3}, while the donor doping density of the ETL was achieved at 1.5 × 10^{22} cm^{-3} doping level. Utilization of palladium as the back contact led to achievement of a higher efficiency. The best device (with GT5 as ETL) achieved a decent power conversion efficiency of (PCE) of above 14%, a fill factor (FF) of 12.84%, a short circuit current density (J_{sc}) of 18.24 mA cm^{-2} and an open circuit voltage (V_{oc}) of 6.04 V. The achieved PCE of above 14% was about 1.93% higher than the experimental value of PCE of 12.22%. Nonetheless, the proposed ETL materials were chosen by mimicking the actual experimental investigation with an aim of giving more insights theoretically. These results will help in further advancement and fabrication of the high performance HTL-free perovskite solar cells (PSCs) for anticipated commercialization.

1. Introduction

Due to the various efforts exhibited to meet the energy demands, perovskite solar cells have emerged as a better option to counter the problem by the conversion of sunlight into electricity compared to other sources of energy such as windmills, biomass, geothermal energy, petrol and nuclear power. The photovoltaic cells have sparked various scientific attention due to their higher power conversion efficiency, cost-effective and portability due to its architecture making it a reliable source of energy [1].

The solar cell development has evolved from the first generation, followed by the second generation and the third generation [2,3]. The first generation involved the crystalline silicon cell including mono-crystalline (mono c-Si), polycrystalline (poly c-Si) and amorphous silicon cells. The second generation involves the thin film solar cells which are rationally engineered to achieve better optical and electronic properties and are classified as amorphous silicon (a-Si) and a-Si/μc-Si, cadmium telluride (Cd-Te); and copper-indium-selenide (CIS) and copper indium-gallium-di selenide (CIGS). The third generation which is the current involves the dye sensitized (DSSC). Perovskite (cell) and the organic (OPV). The third generation of solar cells being made from varieties of materials such as nanomaterials, silicon wires, solar inks using conventional printing press technologies, organic dyes and conductive plastics in order to improve the performance of the solar cell technology making them more efficient, less expensive and nontoxic [2]. Moreover, the categories of solar cells can either be single- or double-layer photovoltaic (PV) systems [4]. Basically, single layer system is a type of solar system or PV system which utilizes a single layer photovoltaic cell to convert sunlight into electricity. Almost all PV cells have a single p-n junction when the photogenerated charges are separated and collected. However, a double layer PV system refers to a system made of two separate layers of photovoltaic cell that are stack on top of each other and usually have a gap or transparent layer in between [5]. The importance of the characteristic double layer PV

* Corresponding author.
E-mail address: nrono@ufh.ac.za (N. Rono).

https://doi.org/10.1016/j.nxener.2025.100245
Received 17 November 2024; Received in revised form 4 January 2025; Accepted 10 January 2025

system is for instance; each layer can be a separate solar system or a model that can be connected in series or parallel [4]. Double layer solar system example includes the bifacial solar panel.

Perovskite solar cell (PSC) shows great potential of being more efficient than silicon based solar cell and for instance, hole transport (HTL)-free based perovskite cells has sparked various scientific attention due to the high cost of the HTL-materials [6,7] and therefore, in to evade the high cost, carbon can be considered as a suitable alternative as the metal carbon contact due to its efficient chemical stability and electrical conductivity [8]. The PSCs device designs play a vital role in performance enhancement. Currently, HTL-free devices offer various advantages over solar cell with HTL component, these includes low cost of production, suppressed recombination losses, reduced toxicity of materials, simpler fabrication process and thereby resulting in enhanced efficiency. Nonetheless, HTL have been investigated and yielded high performance, although for instance Sb_2S_3 [9] is toxic, spiro-OMeTAD on other hand could be expensive and thus, increases the cost of production. Other examples HTL that have been incorporated in PSCs include; P3HT, PEDOT:PSS, PTAA, MoO_3, CFTS [10]. The efficiency of HTL-free photovoltaic cells depends more on the ETL materials as they lead to charge extraction while simultaneously blocking the holes [11]. However, the performance of the HTL-free solar cell is relatively lower than that of perovskite solar cell with the HTL-layer and the back carbon contact [12].

The electron transport layer (ETL) helps to improve the charge extraction and transport holes but on the other hand, unbalanced charge extraction and interface problems commonly occur and therefore, the introduction of interfacial control materials contributes to the improvement of the crystalline quality of perovskite films with increasing grain size and light absorption intensity [13]. Graphitic carbon nitride has been considered as having better optoelectronic properties as it is a metal-free semi-conductor [14,15]. Graphitic carbon nitride (g-C_3N_4) can be affected by limited sunlight absorption, low surface area and fast recombination of photo induced electron-hole pairs and thereby leading to low photocatalytic activity therefore element doping is considered to tune the unique electronic structure and band-gap of g-C_3N_4 [16]. The ZnO doped g-C_3N_4 materials for example, are suitable materials when utilized as ETL because they are an n-type conductors, which can conduct electrons (exhibits high electron mobility), and block the holes thus, separation of excitons. On the other hands, a suitable HTL materials such as spiro-OMETAD and Cu_2O are characterized by having high hole mobility (hence, can transport holes effectively), p-type semiconductor in nature and has ability to block electrons. Other ETL materials such as InS_2, WS_2, SnS_2, [17,18] TiO_2, PCBM, SnO_2 and ZnO [19,20] have been investigated but few studies have reported the used of ZnO doped with g-C_3N_4 in solar cells. The perovskite layer has a structure consisting of (ABX_3) where A represents the organic or inorganic cations such as methylammonium (MA^+) or C_s^+, and B are metallic cations such as Pb^{2+} or Sn^{2+}, while X is a non-metallic anion such as I^-, Br^-; and Cl^- [21,22]. The relatively high performance exhibited by $CH_3NH_3PbI_3$-based solar cells is attributed to the excellent optical absorption, small effective charge carrier masses, dominant point defects that only generate shallow levels, and benign grain boundaries hence reduced recombination of excitons. Moreover, $CH_3NH_3PbI_3$-based devices has gained significant attention due to its higher efficiency, cost-effectiveness and compatibility with the solution processing techniques [23]. Despite the various merits, $CH_3NH_3PbI_3$ suffers from toxicity and stability which can be reduced through use of lead-less or lead-free stable materials and also interface engineering and optimization.

Besides experimental investigation of materials, density functional theory (DFT) has been extensively utilized in the investigation of the structural, physical, electronic, optical, population analysis and thermodynamic properties of materials [24–26]. The obtained parameters regarding a material can suitably be fed into a numerical simulator such as SCAPS-1D and wxAMPS where photovoltaic performance can be evaluated. It is also worth to mention that DFT calculations are relatively time consuming and expensive in the study of the optoelectronic properties of materials, especially, the structural optimization stage, [27–29] when compared to numerical simulations. Nonetheless, the two computational methods have become very handy in the study of solar cells.

It is therefore important to simulate PSC devices to provide more insights that could otherwise be futile experimentally, thus, enhancing their performance. Numerical simulations make it possible for researchers to optimize the performance of the HTL-free solar cell through the adjustments of the various parameters. Moreover, it also aids in reducing the cost of experimental tests through prediction of performance and thus saves on time and resources and also predicts the stability of the solar cell in order to develop long-lasting and dependable solar cells [30].

In this work an HTL-free photovoltaic cell of the configuration; fluorine-doped tin oxide (FTO)/ZnO-g-C_3N_4/$CH_3NH_3PbI_3$/carbon was considered with the aim of obtaining a higher power conversion efficiency (PCE) of the device. The combination of ZnO and graphitic carbon nitride forms a heterojunction that reduces recombination losses and thus enhances the overall performance of the solar cells and thereby making it a promising material in obtaining higher efficiency due to its enhanced charge separation high electron mobility, cost-effectiveness, stability, environmental friendliness and an improved light absorption. Nonetheless, the proposed ETL materials were made by mimicking the actual experimental investigation with the aim of giving more insights theoretically. Simulations were carried out using the solar cell capacitance simulator (SCAPS-1D) to optimize the photovoltaic performance. The performance of the device was compared with the already fabricated device experimentally. Different ETL materials which consist of doped ZnO with g-C_3N_4 was inserted and performance evaluated. The effect of the various parameters affecting the device including the density defect of the absorber (N_t), n-doping of the ETL (N_D) and temperature was considered. The effect of different carbon contacts was also investigated. The PCE current density (J_{sc}), the fill factor (FF) and also the open-circuit voltage (V_{oc}) was discussed This work is envisaged to offer pathways for the fabrication of highly efficient HTL-free based perovskite solar cells in the near future.

2. Computational methodology

In this study HTL-free based perovskite solar cell was considered and simulated using SCAPS-1D software developed by professor Marc Burgelman and his team at the university of Ghent Belgium [31]. The device consists of FTO coating glass/ETL g-C_3N_4/absorber $CH_3NH_3PbI_3$/carbon as shown in Fig. 1. SCAPS-1D aids in the numerical simulation of the photovoltaic device and to solve the semiconductor equations which comprises of the Poisson equation, equations of continuity of holes and electrons [32] and drift-diffusion equation (for both electrons and holes) [33]. The Poisson's, and continuity equations for holes and electrons can be expressed in Eqs. (1)–(3), respectively.

$$\frac{\mathrm{d}}{\mathrm{d}x}\left(\varepsilon(x)\frac{\mathrm{d}\phi}{\mathrm{d}x}\right) = q\left[P(x) - n(x) + N_{\mathrm{d}^+}(x) - N_{a^-}(x) + P_t(x) - n_t(x)\right] \tag{1}$$

$$\frac{\mathrm{d}P_n}{\mathrm{d}t} = G_P - \frac{P_n - P_{n^0}}{\tau_P} - P_n u_P \frac{\mathrm{d}E}{\mathrm{d}x} - u_P E\frac{\mathrm{d}P_n}{\mathrm{d}X} + D_P\frac{\mathrm{d}^2P_n}{\mathrm{d}x^2} \tag{2}$$

$$\frac{dnp}{\mathrm{d}t} = G_n - \frac{n_P - n_{P0}}{\tau_n} - n_P u_n^{\mathrm{d}}\frac{E}{\mathrm{d}x} - u_n E\frac{\mathrm{d}n_P}{dx} + Dp\frac{\mathrm{d}^2n_P}{\mathrm{d}x^2} \tag{3}$$

where q represents the electron charge, G is the rate generation, ϕ is the electrostatic potential, ε is the dielectric permittivity, D represents the diffusion coefficient, E stands for the electric field, $n(x)$ is the number of free electrons, $P(x)$ is the number of free holes, $P_t(x)$is the number of

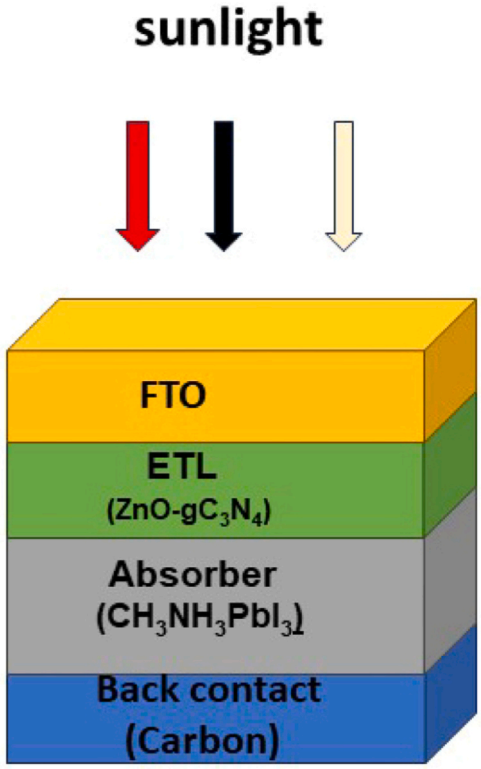

Fig. 1. The device architecture of the HTL-free perovskite solar cell under investigation. HTL = hole transport layer.

trapped holes, $n_t(x)$ is the number of trapped electrons, N_{d^+} represents the concentration of donor ionized doping, N_{a^-} is the concentration of acceptor ionized doping and x stands for the thickness. Meanwhile the drift-diffusion equations for electrons and holes can be expressed in Eqs. (4) and (5), respectively.

$$J_n = q\mu_n n\epsilon + qD_n \partial n \tag{4}$$

$$J_P = q\mu_P n\epsilon + qD_P \partial P \tag{5}$$

In the following drift-diffusion equation, D_n represents the electron diffusion coefficient, D_P is the hole diffusion coefficient, μ_n is the mobility of electrons and $\mu_P$stands for the mobility of hole [34].

The simulation conditions were illumination of AM 1.5G with the power of 100 mW cm^{-2} and a temperature of 300 K. The various input parameters of the device are summarized in Table 1 and Table 2. The work function of the carbon back contact was 5.0 eV [35].

3. Results and discussion

HTL-free based PSC with an architecture FTO/(ZnO-g-C_3N_4)/$CH_3NH_3PbI_3$/carbon was selected and simulations undertaken depending on different values of band gap. The quantum efficiency (QE), current density-voltage (J-V) curve, temperature, density of defect of the absorber, donor density of the ETL the back contact and photovoltaic device parameters including; the (FF), (V_{oc}), (PCE) and (J_{sc}) were considered. Since thickness optimization is crucial in solar cell performance, various layer thickness optimization was performed as the initial step. As an example, the device with GT1 as the ETL was used.

Typically, the thickness of the ETL was adjusted from 1.0 to 0.009 μm keeping the thickness of other layers constant and the best value obtained was 0.05 μm. The thickness of the FTO was thereafter varied from 1.2 to 0.001 μm maintaining other layer's value constant and achieved the best value as 0.05 μm. The thickness of the absorber was again varied from 2.0 to 0.1 μm and the optimum value obtained was 0.3 μm, while, maintaining the other component's thickness constant. The same procedure was conducted in other devices to attain an optimum value of layers thickness. Therefore, for device with the GT3 as ETL material was optimized sequentially and obtained the best value of the ETL, FTO and absorber as 0.001, 0.001 and 0.3 μm, respectively. Finally, the GT5-based device was afterward optimized sequentially and thickness value of the ETL, FTO and the absorber varied and obtained the best value as 0.001, 0.001, 0.3 μm, correspondingly. Table 3 shows the performance of the devices with different band gap materials as measured from the experimental work of ref [37].

Table 1
Different simulation input parameters of the modeled device

Parameter	FTO [36]	ZnO [35]	$CH_3NH_3PbI_3$ (absorber) [35]
Band gap, E_g (eV)	3.5	Varied	1.63
Affinity, χ (eV)	4.0	4.26	4.10
Dielectric permittivity (relative), ε_r	9.0	9	9.6
Effective density of state at CB, N_c (cm^{-3})	2.2×10^{18}	2.8×10^{18}	2.2×10^{18}
Effective density of state at VB, N_v (cm^{-3})	1.8×10^{19}	1.8×10^{19}	1.8×10^{19}
Mobility of electrons, μ_n ($cm^2\ V^{-1}\ s^{-1}$)	20.0	200	0.017
Mobility of holes, μ_p ($cm^2\ V^{-1}\ s^{-1}$)	10.0	5	0.059
Density of n-type doping, N_D (cm^{-3})	1.0×10^{19}	1.5×10^{17}	1.0×10^{12}
Density of p-type doping, N_A (cm^{-3})	0.0	0.0	1.0×10^{12}
Density of defects, N_t (cm^{-3})	0.0	1.0×10^{16}	1.0×10^{15}

Table 2
Basic input parameters of the various ETL (ZnO-g-C_3N_4) materials from ref. [37]

Parameter	GT1	GT3	GT5
E_g (eV)	3.06	3.10	2.97
χ (eV)	4.26	4.26	4.26
ε_r	9.0	9.0	9.0
N_c (cm^{-3})	2.0×10^{18}	2.0×10^{18}	2.0×10^{18}
N_v (cm^{-3})	1.8×10^{19}	1.8×10^{19}	1.8×10^{19}
μ_n ($cm^2\ V^{-1}\ s^{-1}$)	200	200	200
μ_p ($cm^2\ V^{-1}\ s^{-1}$)	5	5	5
N_D (cm^{-3})	1.5×10^{17}	1.5×10^{17}	1.5×10^{17}
N_A (cm^{-3})	0.0	0.0	0.0
N_t (cm^{-3})	1.0×10^{16}	1.0×10^{16}	1.0×10^{16}

ETL = electron transport layer.

Table 3
Photovoltaic performance of the devices with pure ZnO, GT1, GT3 and GT5 ETL materials

Sample	V_{oc} (V)	J_{sc} (mA cm^{-2})	FF (%)	PCE (%)
ZnO	0.75	16.84	50.05	6.33
GT1	0.75	16.84	50.05	6.33
GT3	0.72	17.14	60.27	7.46
GT5	0.72	17.15	60.27	7.46

ETL = electron transport layer; FF = fill factor; J_{sc} = current density; PCE = power conversion efficiency; Voc = open-circuit voltage.

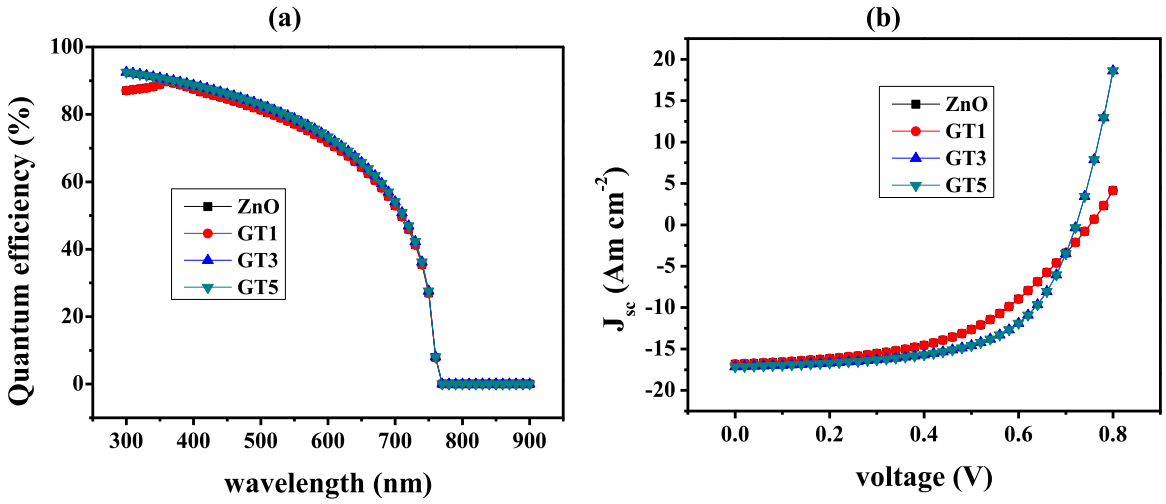

Fig. 2. The quantum efficiency versus wavelength and current density versus voltage for the devices with pure ZnO, GT1, GT3 and GT5 ETL materials. ETL = electron transport layer.

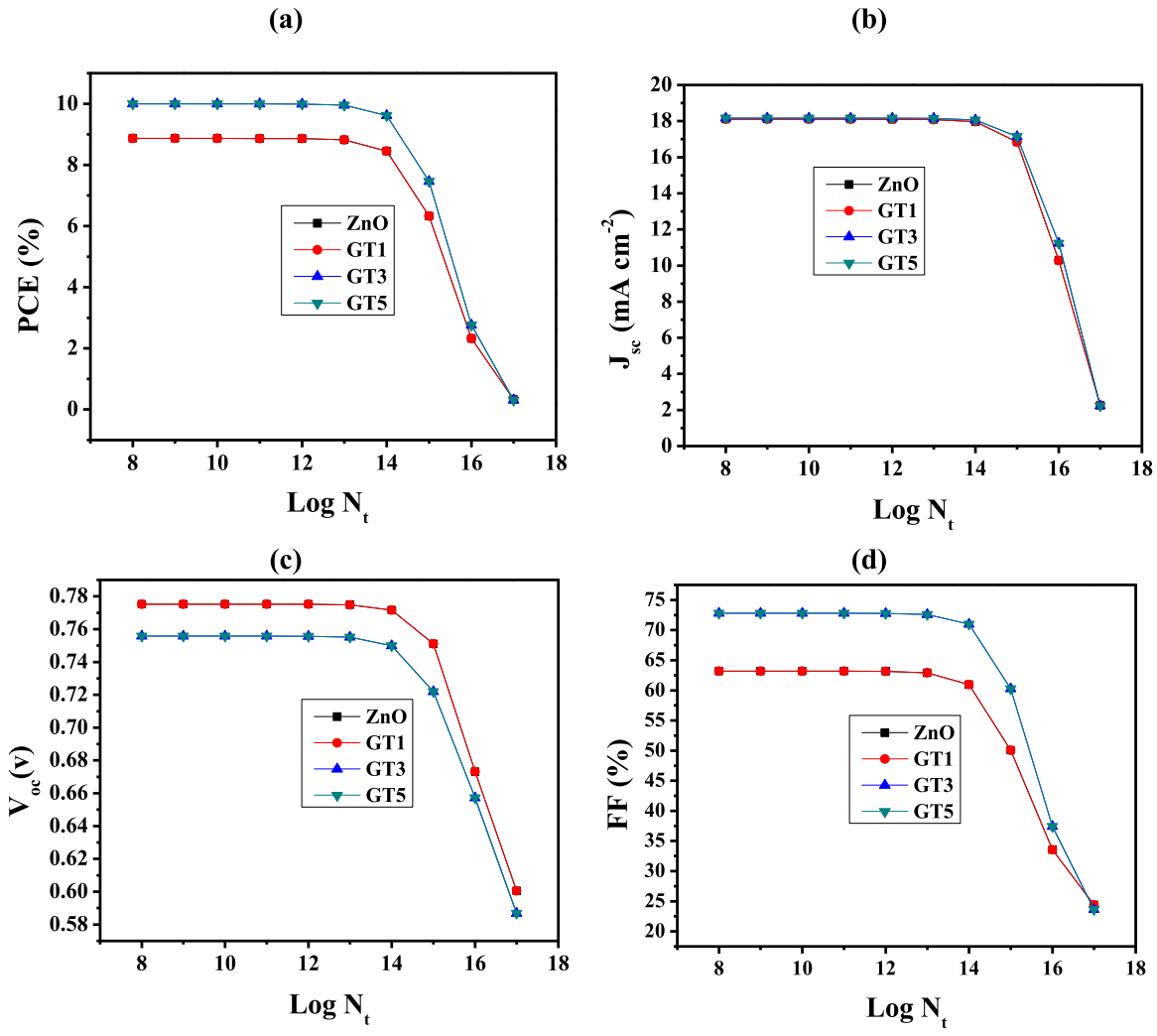

Fig. 3. The performances of the devices with pure ZnO, GT1, GT3 and GT5 ETL materials as a function of increasing the density of the defect of the absorber. (a) PCE, (b) J_{sc}, (c) V_{oc} and (d) FF. ETL = electron transport layer; FF = fill factor; J_{sc} = current density; PCE = power conversion efficiency; V_{oc} = open-circuit voltage.

3.1. Quantum efficiency and J-V curves

In order to attain a higher power conversion efficiency, the Quantum efficiency of the device was reviewed to determine the percentage of incoming photons transformed into charge carriers. From Fig. 2(a) the device reveals a quantum efficiency of about 86% at 300 nm and thereafter a slight increase to 90% for pure ZnO and GT1 with the best value at about 360 nm. The GT3- and GT5-based devices

Table 4
Optimized extracted photovoltaic parameters of devices with different ETL materials as a function of changing absorber density of defects

Sample	V_{oc} (V)	J_{sc} (mA cm^{-2})	FF (%)	PCE (%)
ZnO	0.78	18.10	63.17	8.87
GT1	0.78	18.10	63.17	8.87
GT3	0.78	18.17	72.77	9.99
GT5	0.78	18.17	72.77	9.99

ETL = electron transport layer; FF = fill factor; J_{sc} = current density; PCE = power conversion efficiency; Voc = open-circuit voltage.

Table 5
Effect of the n-doping of the ETL for the devices with pure ZnO, GT1, GT3 and GT5 materials

Sample	V_{oc} (V)	J_{sc} (mA cm^{-2})	FF (%)	PCE (%)
ZnO	0.75	18.18	73.76	10.09
GT1	0.75	18.18	73.76	10.09
GT3	0.75	18.18	73.71	10.08
GT5	0.75	18.18	73.71	10.08

ETL = electron transport layer; FF = fill factor; J_{sc} = current density; PCE = power conversion efficiency; Voc = open-circuit voltage.

exhibited a quantum efficiency of about 93% implying that the device generates a higher amount of current when irradiated by photons of a particular wavelength. Simultaneous decrease in the quantum efficiency is then observed to about 700 nm and later declines and levels off from about 750–900 nm as the device does not obtain light. From Fig. 2(b), the voltage was varied from 0.0 to 0.8 V which shows a slight increase in current generation from 0.0 to about 0.5 V and eventually a further increase up to 0.8 V as the passive oxide layer breaks [38] with increasing voltage. The device attains a high current generation at 0.8 V.

3.2. *Effect of changing the density of defect of the absorber on performance*

Essentially, high concentrations of the defect causes a higher recombination due to the generation of pinholes, higher degradation rate of the film, reduced stability and reduced performance of the device [39]. The density of the defect of the absorber therefore plays an essential role on the performance of the devices. Fig. 3 shows the variations of the density defect of the absorber on the photovoltaic performance of the device. The density of the defect was varied from 1.0 × 10^{8} to 1.0 × 10^{17} cm^{-3} for devices with different ETL materials. From Fig. 3(a) the density defect exhibits a higher PCE from 1.0 × 10^{8} to 1.0 × 10^{13} cm^{-3} and finally a decrease in performance which could be probably due to an increase in trap layers at the perovskite film at higher density defect thereby resulting in increased non-radioactive recombination [40]. The J_{sc} (Fig. 3b) remains constant and thereafter, decreases steadily and this was attributed maybe due to the existence of more number of the trap sites [41]. Fig. 3(c) reveals that the V_{oc} remains constant as density of defect increases and later a decrease which could be due to recombination of charge carriers thereby hindering its

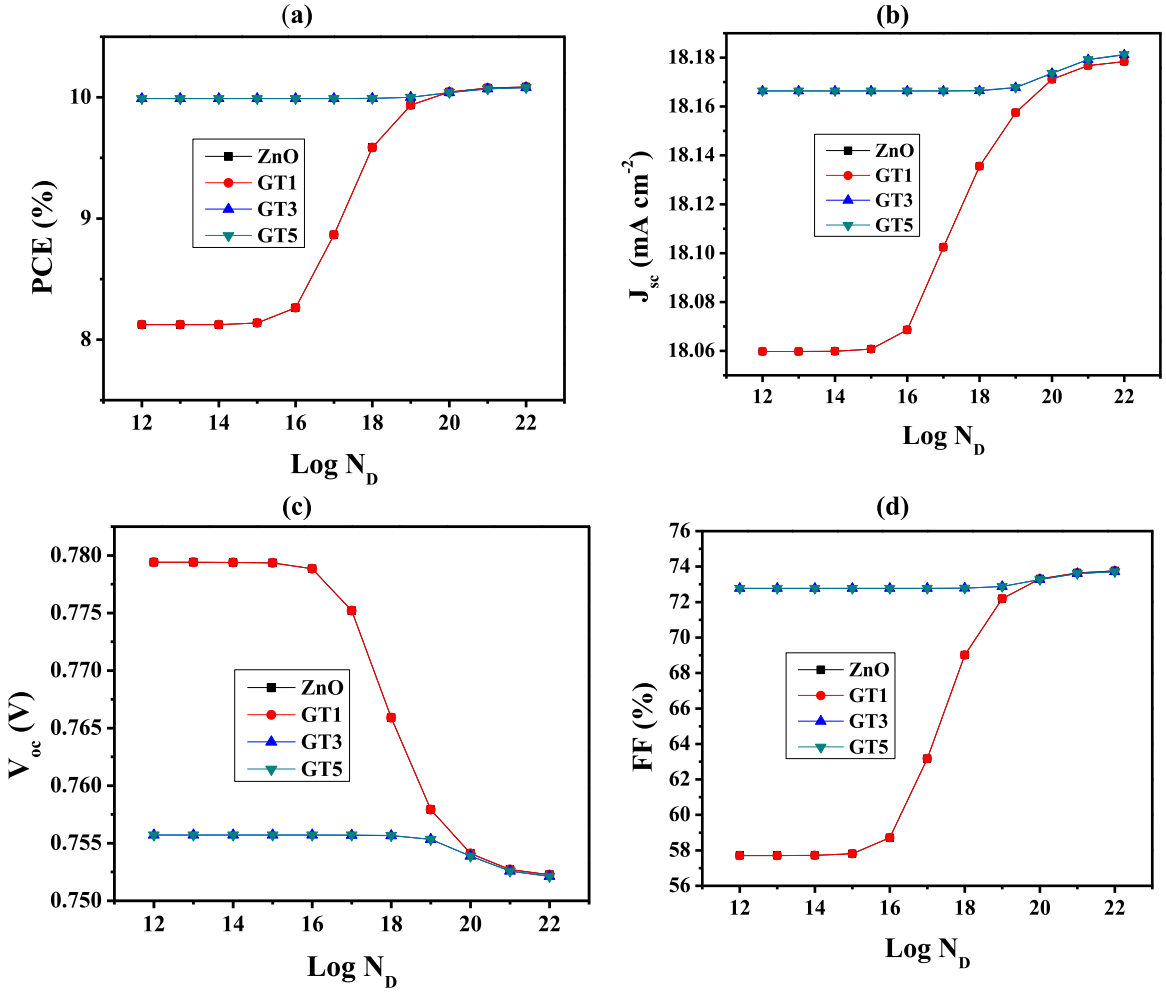

Fig. 4. The performances of the devices with pure ZnO, GT1, GT3 and GT5 materials as a function of increasing n-doping of the ETL. (a) PCE, (b) J_{sc}, (c) V_{oc} and (d) FF. ETL = electron transport layer; FF = fill factor; J_{sc} = current density; PCE = power conversion efficiency; V_{oc} = open-circuit voltage.

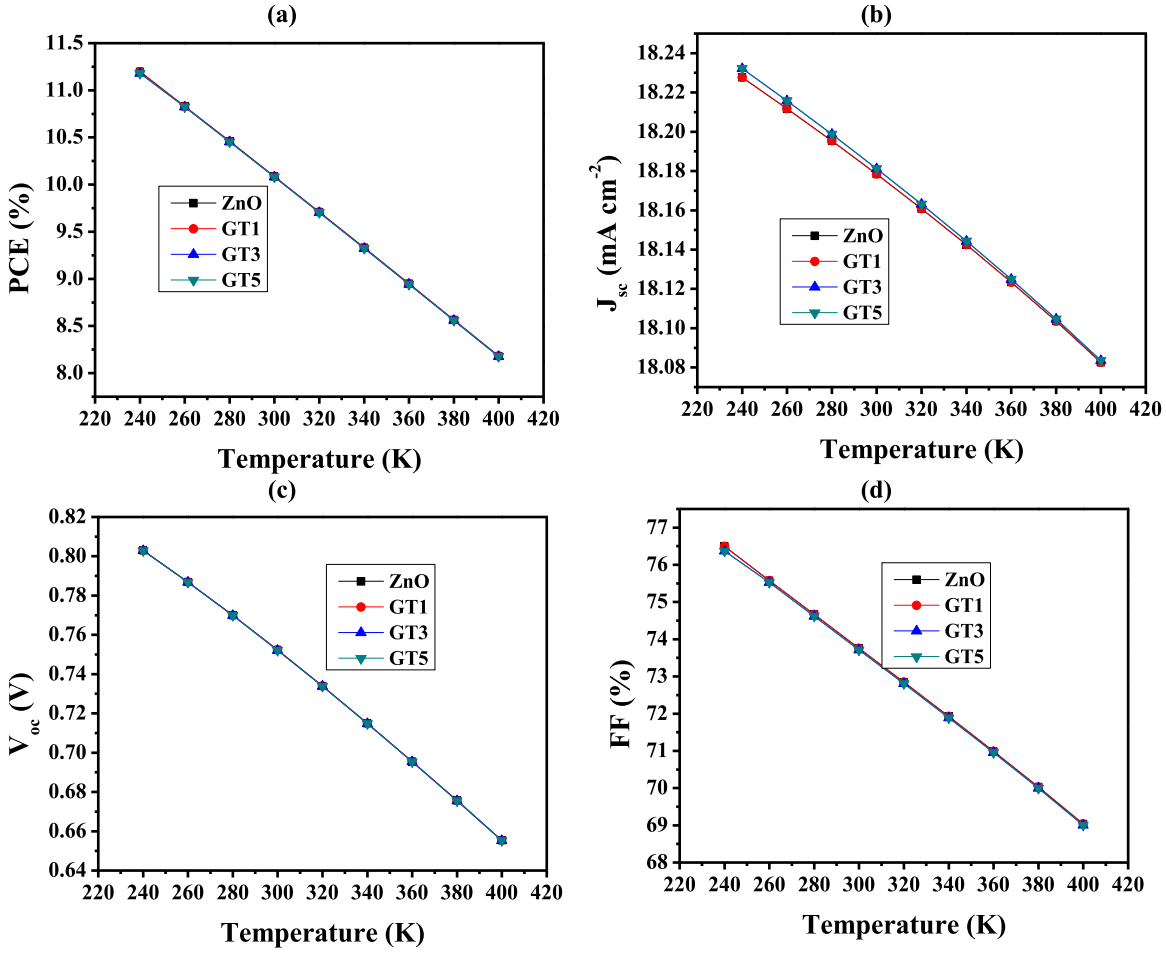

Fig. 5. The performance for devices with pure ZnO, GT1, GT3 and GT5 ETL materials as a function of increasing temperature. (a) PCE, (b) J_{sc}, (c) V_{oc} and (d) FF. ETL = electron transport layer; FF = fill factor; J_{sc} = current density; PCE = power conversion efficiency; V_{oc} = open-circuit voltage.

Table 6
Effect of temperature on photovoltaic performance of the devices with pure ZnO, GT1, GT3 and GT5 materials at an operational temperature of 300 K

Sample	V_{oc} (V)	J_{sc} (mA cm^{-2})	FF (%)	PCE (%)
ZnO	0.80	18.23	76.43	11.20
GT1	0.80	18.23	76.43	11.20
GT3	0.80	18.23	76.31	11.18
GT5	0.80	18.23	76.71	11.18

FF = fill factor; J_{sc} = current density; PCE = power conversion efficiency; Voc = open-circuit voltage.

ability to convert sunlight to electricity [42]. From Fig. 3(d), the FF remains constant as the density defect increases from 1.0 × 10^{8} to 1.0 × 10^{13} cm^{-3} and thereafter a decrease possibly due to the increase in resistance charge pathway [42]. Nonetheless, the optimal density of defect was kept at 1.0 × 10^{11} cm^{-3} level for ZnO and GT1 while GT3 and GT5 was maintained at 1.0 × 10^{12} cm^{-3} level.

Table 4 summarizes the best the photovoltaic performance of the different devices with different ETL materials.

3.3. Impact of the donor density of the ETL

The n-doping of the ETL plays a critical role in the improvement of the performance of the solar cell and therefore application of the simulation has greatly improved the efficiency of the devices [43]. Fig. 4 shows the effect of the variations of donor density of the ETL on the performance of the devices. The n-doping of the ETL was varied from 1.5 × 10^{12} to 1.5 × 10^{22} cm^{-3} for the different band gap materials. The n-doping of the ETL attributed to the increased power conversion efficiency of the devices thus improving its ability to convert sunlight to electricity. From Fig. 4(a) the increase in donor density of the ETL for ZnO and GT1 results in a constant value of PCE from 1.5 × 10^{12} to about 1.5 × 10^{15} cm^{-3} which could be due to increased conductivity [3] and thereafter an increase in PCE as the donor density increased to 1.5 × 10^{20} cm^{-3} followed by a constant value of PCE. The device with GT3 and GT5 as ETL materials shows a constant value of PCE of over 10% from 1.5 × 10^{12} to 1.5 × 10^{22} cm^{-3} which could be attributed to the improved separation efficiency revealing that the PCE was not affected by the change in the doping concentration. Fig. 4(b) showed that, for ZnO and GT1 devices, the current density remains constant from 1.5 × 10^{12} to 1.5 × 10^{14} cm^{-3} followed by an increase in current density as the donor density increased to 1.5 × 10^{21} cm^{-3} and thereafter a slight increase to 1.5 × 10^{22} cm^{-3} probably because the less thickness of the FTO (0.05 eV) allows more light to be transmitted to the absorber [41]. The V_{oc} (Fig. 4c) for ZnO and GT1 device, remains constant from 1.5 × 10^{12} to 1.5 × 10^{15} cm^{-3} as the recombination resistance neither decreased nor increased [44] and finally a decrease to 1.5 × 10^{22} cm^{-3}. GT3 and GT5 unveiled a steady value of the V_{oc} from 1.5 × 10^{12} to 1.5 × 10^{18} cm^{-3} as the recombination rate is not affected and thereafter, an increase before reaching to saturation at 1.5 × 10^{22} cm^{-3}. From Fig. 4(d) the FF remains constant from 1.5 × 10^{12} to 1.5 × 10^{15} cm^{-3} and thereafter increases before reaching to a constant value at 1.5 × 10^{21} cm^{-3} probably due to reduction in series resistance, [44] thus, achieving an optimum value of 76.43%. Meanwhile, GT3 and GT5-based devices were not affected by changing the doping concentration

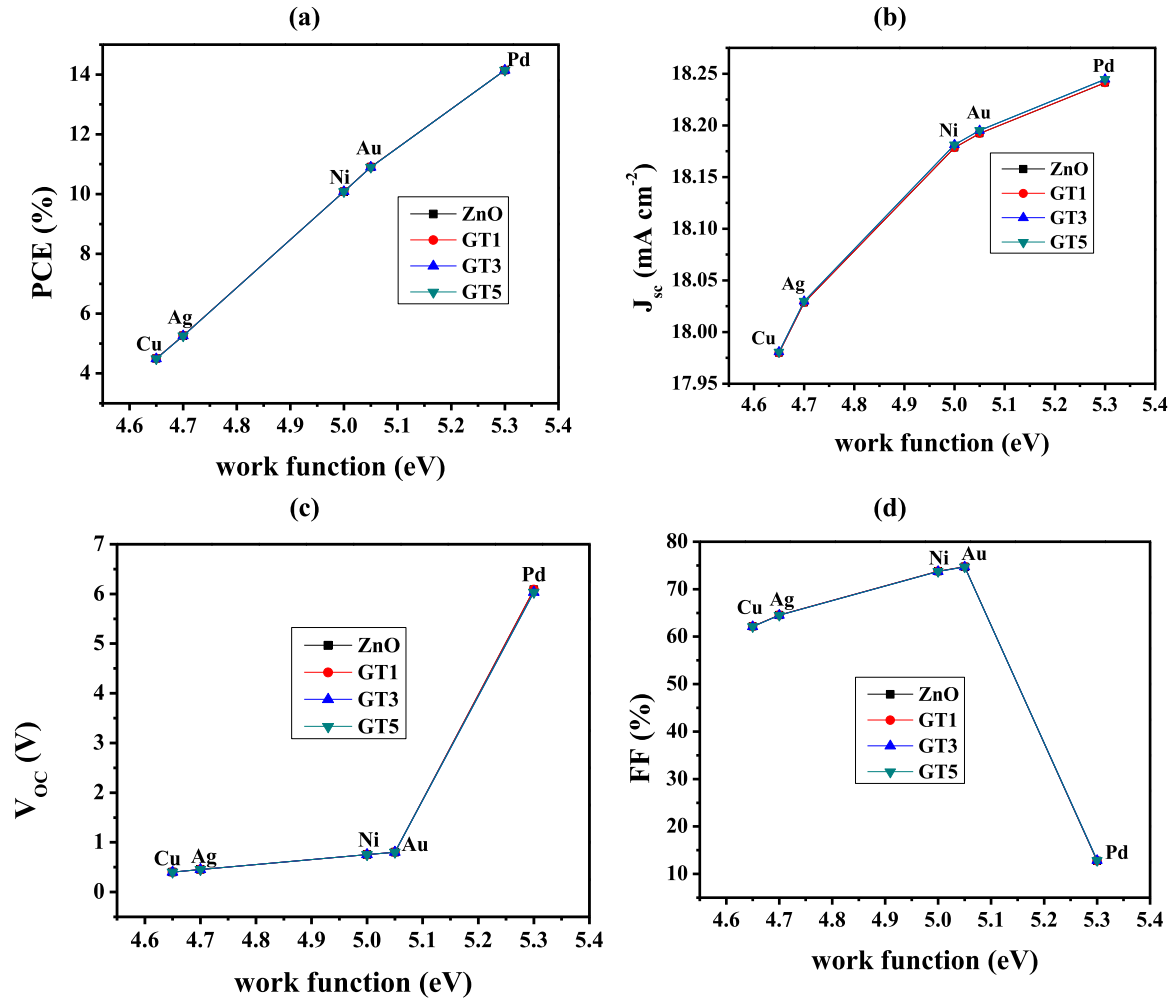

Fig. 6. The performances of the devices with pure ZnO, GT1, GT3 and GT5 as ETL materials as a function of increasing the work functions. (a) PCE, (b) J_{sc}, (c) V_{oc} and (d) FF. ETL = electron transport layer; FF = fill factor; J_{sc} = current density; PCE = power conversion efficiency; V_{oc} = open-circuit voltage.

Table 7
Photovoltaic performance for devices with pure ZnO, GT1, GT3 and GT5 materials and Pd back contact

Sample	V_{oc} (V)	J_{sc} (mA cm^{-2})	FF (%)	PCE (%)
ZnO	6.09	18.24	12.74	14.14
GT1	6.09	18.24	12.74	14.14
GT3	6.03	18.24	12.84	14.14
GT5	6.04	18.24	12.84	14.14

FF = fill factor; J_{sc} = current density; PCE = power conversion efficiency; Voc = open-circuit voltage.

from 1.5 × 10^{12} to 1.5 × 10^{19} cm^{-3} and thereafter it experienced a slight increase to 1.5 × 10^{22} cm^{-3}. The optimum donor density of the ETL was maintained at 1.5 × 10^{22} cm^{-3} in order to improve the stability efficiency, the overall performance of the devices and ensure cost-effective devices at the industrial level (Table 5).

3.4. Temperature variation and the effect on performance

The temperature increase adversely affects the performance of the solar cell thereby leading to its inefficiency at higher temperature due to increased recombination rates [45] but also more effective at lower temperatures. In our case, simulations were conducted at 300 K but in order to obtain the effect of the operating temperature on the devices, the temperature was varied from 240 to 400 K. The devices achieved a higher efficiency at 240 K.

From Fig. 5(a) the continued increase in the temperature from 240 to 400 K led to a decrease in efficiency which could be due to the high electron photon interaction. The J_{sc} (Fig. 5b) decreases with increase in

Table 8
Performance evaluation of different devices with or without HTL materials

Device configuration	Experimental/ simulation	V_{oc} (V)	J_{sc} (mA cm^{-2})	FF (%)	PCE (%)	References
FTO/TiO_2/$CH_3NH_3PbI_3$/spiro-OMeTAD/Au	simulation	1.48	15.15	90.91	20.34	[49]
FTO/IGZO/$CH_3NH_3PbI_3$/spiro-OMeTAD/Au	simulation	5.32	25.55	14.68	19.95	[50]
FTO/ZnSe/$CH_3NH_3PbI_3$/C	simulation	1.25	24.77	86.29	26.76	[51]
FTO/g-C_3N_4/$CH_3NH_3PbI_3$/C	experimental	0.79	15.36	0.64	12.22	[37]
FTO/g-C_3N_4/$CH_3NH_3PbI_3$/C	simulation	6.04	18.24	12.84	14.14	This work

FF = fill factor; HTL = hole transport layer; J_{sc} = current density; PCE = power conversion efficiency; Voc = open-circuit voltage.

temperature which could be attributed to better absorption rate of photons therefore leading to more generation of excitations for the different band gap materials. From Fig. 5(c), the V_{oc} decreases with increase in temperature possibly due to the electron hole recombination leading to decreased efficiency for the different band gap materials. The FF (Fig. 5d) decreased with increase in temperature which may be due to increased series resistance and decreased shunt resistance [46] for the different band gap materials.

Nonetheless, Table 6 shows the efficiencies of the devices at optimal operational temperature of 300 K.

3.5. Effect of utilization of different back contacts on device performances

The back contact in an HTL-free perovskite eliminates the need for the HTL in methylammonium lead iodide due to the suitable barrier height of electrons by blocking the electrons while collecting the holes [47]. In order to optimize the performance of the devices, a suitable back contact material was investigated through the work functions of the back contact materials. The carbon back contact was adjusted from various work functions such as Pd (5.3 eV), Ni (5.0 eV), Ag (4.7 eV), Au (5.05 eV), and Cu (4.65 eV) [3]. From Fig. 6(a) increase in the work function results in an increase in PCE possibly due to better alignment of the energy levels at the interface between the back contact and the perovskite layer [46]. Palladium obtains a higher efficiency of 14.14%, gold (Au) garnered a PCE of 10.9% while nickel (Ni) obtained 10.09% whereas silver (Ag) and copper (Cu) obtained a relatively lower efficiency. Palladium, gold and nickel are preferred as the best back contact due to their higher performance, but Au is expensive and therefore Pd and Ni could be used in place of Au as they are less expensive. The increased work function (Fig. 6b) resulted in an increased current density and palladium obtained a higher value. Fig. 6(c) reveals that V_{oc} slightly increased with increase in the work function from 4.65 to 5.05 eV and thereafter a drastic increase to 5.3 in the work function of palladium possibly due to the good alignment of the interfacial energy and the reduction of the recombination [48] leading to a higher built-in potential. From Fig. 6(d), it shows that the increase in the work function attributed to an increase in FF and thereby Au (5.05 eV) obtaining a higher value of the fill factor followed by a drastic decrease in the FF until 5.3 eV of palladium. From these results, it can be resolved that optimization of the back contact improves the efficiency of the devices (Table 7).

3.6. Comparative study

In order to evaluate the performance of our modeled FTO/g-C_3N_4/$CH_3NH_3PbI_3$/C device, other similar devices were compared with it as presented in Table 8. Generally, the HTL-based solar cell showed a higher efficiency than HTL-free based devices as depicted in Table 8. Despite the relatively higher performance exhibited by HTL-based devices, it requires higher cost of fabrication due to the incorporation of the HTL layer. Although, FTO/ZnSe/$CH_3NH_3PbI_3$/C configuration, showed higher PCE in the HTL-free based devices, ZnSe is relatively more expensive when compared to g-C_3N_4 or ZnO. Therefore, the incorporation of the g-C_3N_4 will lower the cost of production significantly.

4. Conclusions

In this paper, the devices with an architecture FTO/ZnO-g-C_3N_4/$CH_3NH_3PbI_3$/carbon was simulated using SCAPS-1D. The modeled device achieved a higher PCE of 14.1% than the previous experimental works that achieved a PCE of 12.22% with an increase of 1.93%. The various parameters such, density of the defect of the absorber, n-doping of the ETL, temperature and the back contact plays a crucial role in improving the performance of the HTL-free perovskite solar cell and thereby attributed to a significant increase in the power conversion efficiency. Simulations were performed and thicknesses of various layers optimized and consequently attributed to the increase in the performance. The density of the defect of the absorber obtained was an optimal value of 1.0×10^{11} cm^{-3} for devices with ZnO and GT1, while for GT3 and GT5 devices, the density level of 1.0×10^{12} cm^{-3} was sufficient. The n-doping of the ETL was maintained at an optimum value of 1.0×10^{22} cm^{-3}. The devices were more stable at 240 K attaining an efficiency of 11.20% for ZnO and GT1, while GT3 and GT5 obtained a slightly lower efficiency of 11.18%. Remarkably, palladium, gold and nickel were preferred as the best back contacts with palladium obtaining the supreme performance and hence, Au which is expensive can be suitably replaced with Pd and Ni. The best device (GT5-based device) thickness of the absorber and the ETL was maintained at 300 and 1.00 nm, respectively and a more stable device ultimately achieved a PCE of over 14.14% with a FF of 12.84%, a J_{sc} of 18.24 mA cm^{-2} and a V_{oc} of 6.04 V with palladium utilized as the back contact. These results will exhibit an aid in the further fabrication of the HTL-free solar cell in order to obtain a significantly higher efficiency.

Declaration of Competing Interest

The authors declare that they have no known competing financial interests or personal relationships that could have appeared to influence the work reported in this paper.

Acknowledgments

The authors are grateful for the partial/full financial support provided by the National Research Foundation of South Africa (NRF) (grant number: 150863) and the Govan Mbeki Research and Development Center (GMRDC) at the University of Fort Hare. J-K is also grateful to the department of Basic Sciences, Tharaka University, Kenya. C.C.A and N.R. is appreciative to African Laser Center Research (ALCR) Grant (CSIR Reference: HLHA25X task ALC-R006). Finally, J.K and N.R. also thanks Professor Marc Burgelman of the University of Gent, Belgium, for granting access to the SCAPS-1D simulation software.

References

[1] M.H. Ahmadi, M. Ghazvini, M. Alhuyi Nazari, M.A. Ahmadi, F. Pourfayaz, G. Lorenzini, T. Ming, Renewable energy harvesting with the application of nanotechnology: a review, Int. J. Energy Res. 43 (2019) 1387–1410, https://doi.org/10.1002/er.4282.

[2] K. Ranabhat, L. Patrikeev, A.Ae Revina, K. Andrianov, V. Lapshinsky, E. Sofronova, An introduction to solar cell technology, J. Appl. Eng. Sci. 14 (2016) 481–491, https://doi.org/10.5937/jaes14-10879.

[3] N. Rono, An Experimental Study of Graphitic Carbon Nitride-Based Materials and Selected Metal-Based Semiconductors in Organic Solar Cells Combined with a Computational Study of Perovskite Solar Cells, School of Chemistry and Physics, University fo KwaZulu-Natal, South Africa: Durban, 2023.

[4] P. Sharma, T. Harinarayana, Enhancement of energy generation from two layer solar panels, Int. J. Energy Environ. Eng. 3 (2012) 12, https://doi.org/10.1186/2251-6832-3-12.

[5] BRSolarGroup, The difference between single glass solar modules and double glass solar modules. 2024: Yangzhou City, Jiangsu Province, P.R.China.

[6] A. Mei, X. Li, L. Liu, Z. Ku, T. Liu, Y. Rong, M. Xu, M. Hu, J. Chen, Y. Yang, A hole-conductor–free, fully printable mesoscopic perovskite solar cell with high stability, Science 345 (2014) 295–298, https://doi.org/10.1126/science.1254763.

[7] K. Ke, K.K. Kondamareddy, F. Gao, X. Zhang, X. Yuan, Fabrication of highly efficient and stable hole-transport material-free perovskite solar cells through morphology and interface engineering: full ambient process, Energy Technol. 7 (2019) 1900446, https://doi.org/10.1002/ente.201900446.

[8] L. Bokobza, J.-L. Bruneel, M. Couzi, Raman spectra of carbon-based materials (from graphite to carbon black) and of some silicone composites, J. Carbon Res. 1 (2015) 77–94, https://doi.org/10.3390/c1010077.

[9] B. Islam, A. Hosen, T.M. Khan, M.F. Rahman, M.H. Rahman, M.S. Islam, S.R.A. Ahmed, Simulating the effect of inserting Sb_2S_3 as hole transport layer on sns-based thin-film solar cells, J. Electron. Mater. (2024) 1–14, https://doi.org/10.1002/adts.202400360.

[10] M.F. Rahman, M.A.I. Islam, M. Chowdhury, L.B. Farhat, S. Ezzine, A.S. Islam, Efficiency improvement of $CsSnI_3$ based heterojunction solar cells with P3HT HTL: a numerical simulation approach, Mater. Sci. Eng.: B 307 (2024) 117524, https://doi.org/10.1016/j.mseb.2024.117524.

[11] H. Wei, J. Xiao, Y. Yang, S. Lv, J. Shi, X. Xu, J. Dong, Y. Luo, D. Li, Q. Meng, Free-standing flexible carbon electrode for highly efficient hole-conductor-free perovskite solar cells, Carbon 93 (2015) 861–868, https://doi.org/10.1016/j.carbon.2015.05.042.

[12] S. Ijaz, E. Raza, Z. Ahmad, H. Mehmood, M. Zubair, M.Q. Mehmood, Y. Massoud, A numerical approach to optimize the performance of HTL-free carbon electrode-based perovskite solar cells using organic ETLs, Heliyon 10 (2024) e29091, https://doi.org/10.1016/j.heliyon.2024.e29091.

[13] W. Cao, J. Zhang, K. Lin, L. Qiu, J. Li, Y. Dong, J. Wang, D. Xia, R. Fan, Y. Yang, Enhanced charge transport and interface passivation in efficient perovskite solar cells using sulfur-doped graphite carbon nitride-modified SnO_2-based electron transport layers, Sol. RRL 5 (2021) 2100058, https://doi.org/10.1002/solr.202100058.

[14] M. Mousavi, A. Habibi-Yangjeh, S.R. Pouran, Review on magnetically separable graphitic carbon nitride-based nanocomposites as promising visible-light-driven photocatalysts, J. Mater. Sci.: Mater. Electron. 29 (2018) 1719–1747, https://doi.org/10.1007/s10854-017-8166-x.

[15] T. Fidan, M. Torabfam, Q. Saleem, C. Wang, H. Kurt, M. Yüce, J. Tang, M.K. Bayazit, Functionalized graphitic carbon nitrides for environmental and sensing applications, Adv. Energy Sustain. Res. 2 (2021) 2000073, https://doi.org/10.1002/aesr.202000073.

[16] L. Jiang, X. Yuan, Y. Pan, J. Liang, G. Zeng, Z. Wu, H. Wang, Doping of graphitic carbon nitride for photocatalysis: a review, Appl. Catal. B: Environ. 217 (2017) 388–406, https://doi.org/10.1016/j.apcatb.2017.06.003.

[17] M.S. Reza, M.F. Rahman, M.S. Reza, M.R. Islam, U.U. Rehman, A.R. Chaudhry, A. Irfan, Rubidium based new lead free high performance perovskite solar cells with SnS_2 as an electron transport layer, Mater. Today Commun. 39 (2024) 108714, https://doi.org/10.1016/j.mtcomm.2024.108714.

[18] M.S. Reza, M.F. Rahman, A. Kuddus, M.K. Mohammed, D. Pal, A. Ghosh, M.R. Islam, S. Bhattarai, I.A. Shaaban, M. Amami, Design and optimization of high-performance novel $RbPbBr_3$-based solar cells with wide-band-gap s-chalcogenide electron transport layers (ETLs), ACS Omega 9 (2024) 19824–19836, https://doi.org/10.1021/acsomega.3c08285.

[19] M.H. Ishraq, M.R. Kabir, M. Tarekuzzaman, M.F. Rahman, M. Rasheduzzaman, M.Z. Hasan, ETL and HTL engineering in $CH_3NH_3PbBr_3$ perovskite for stable and efficient performance photovoltaic devices applications using SCAPS-1D, Adv. Theory Simul. 7 (2024) 2400360, https://doi.org/10.1002/adts.202400360.

[20] M.K. Hossain, G.F.I. Toki, A. Kuddus, M.H.K. Rubel, M.M. Hossain, H. Bencherif, M.F. Rahman, M.R. Islam, M. Mushtaq, An extensive study on multiple ETL and HTL layers to design and simulation of high-performance lead-free $CsSnCl_3$-based perovskite solar cells, Sci. Rep. 13 (2023) 2521, https://doi.org/10.1038/s41598-023-28506-2.

[21] M.S. Mkehlane, Electroanalysis of organo-chalcogenic perovskite nanomaterials. 2017.

[22] Y. Li, Design and Synthesis of Perovskite Materials for Photocatalytic and Photovoltaic Applications, Hong Kong Baptist University, 2022.

[23] D. Dastan, M.K. Mohammed, R.Sh Alnayli, S. M. Majeed, D.S. Ahmed, A.K. Al-Mousoi, R. Pandey, M.K. Hossain, S. Bhattarai, B.A. Al-Asbahi, Achieving well-oriented $FAPbI_3$ perovskite photovoltaics by cyclohexane modification, Langmuir 40 (2024) 7560–7568, https://doi.org/10.1021/acs.langmuir.4c00136.

[24] M.M. Rahaman, K.M. Hossain, M.H.K. Rubel, A.A. Islam, S. Kojima, Alkaline-earth metal effects on physical properties of ferromagnetic AVO_3 (A = Ba, Sr, Ca, and Mg): density functional theory insights, ACS Omega 7 (2022) 20914–20926, https://doi.org/10.1021/acsomega.2c01630.

[25] M. Rubel, M. Hossain, M.K. Hossain, K. Hossain, A. Khatun, M. Rahaman, M.F. Rahman, M. Hossain, J. Hossain, First-principles calculations to investigate structural, elastic, electronic, thermodynamic, and thermoelectric properties of $CaPd_3B_4O_{12}$ (B = Ti, V) perovskites, Results Phys. 42 (2022) 105977, https://doi.org/10.1016/j.rinp.2022.105977.

[26] M.K. Hossain, S. Islam, M.N. Sakib, M.S. Uddin, G.F. Toki, M.H. Rubel, J. Nasrin, S.H. Shahatha, M. Mohammad, A.A. Alothman, Exploring the optoelectronic and photovoltaic characteristics of lead-free Cs_2TiBr_6 double perovskite solar cells: a DFT and SCAPS-1D investigations, Adv. Electron. Mater. (2024) 2400348, https://doi.org/10.1002/aelm.202400348.

[27] S. Bouhmaidi, M.B. Uddin, R.K. Pingak, S. Ahmad, M.H.K. Rubel, A. Hakamy, L. Setti, Investigation of heavy thallium perovskites $TlGeX_3$(X = Cl, Br and I) for optoelectronic and thermoelectric applications: a DFT study, Mater. Today Commun. 37 (2023) 107025, https://doi.org/10.1016/j.mtcomm.2023.107025.

[28] M.K. Hossain, M.K. Mohammed, R. Pandey, A. Arnab, M. Rubel, K. Hossain, M.H. Ali, M.F. Rahman, H. Bencherif, J. Madan, Fuels, numerical analysis in DFT and SCAPS-1D on the influence of different charge transport layers of $CsPbBr_3$ perovskite solar cells, Energy Technol. 37 (2023) 6078–6098, https://doi.org/10.1021/acs.energyfuels.3c00035.

[29] M.K. Hossain, M.H.K. Rubel, G.I. Toki, I. Alam, M.F. Rahman, H. Bencherif, Effect of various electron and hole transport layers on the performance of $CsPbI_3$-based perovskite solar cells: a numerical investigation in DFT, SCAPS-1D, and wxAMPS frameworks, ACS Omega 7 (2022) 43210–43230, https://doi.org/10.1021/acsomega.2c05912.

[30] M.K. Hossain, G.I. Toki, I. Alam, R. Pandey, D. Samajdar, M.F. Rahman, M.R. Islam, M. Rubel, H. Bencherif, J. Madan, Numerical simulation and optimization of a $CsPbI_3$-based perovskite solar cell to enhance the power conversion efficiency, N. J. Chem. 47 (2023) 4801–4817, https://doi.org/10.1039/D2NJ06206B.

[31] M. Mahiny, S. Ahmadi-Kandjani, B. Olyaeefar, Classical modeling of extrinsic degradation in polycrystalline perovskite solar cells; defect induced degradation, Sol. Energy Mater. Sol. Cells 261 (2023) 112500, https://doi.org/10.1016/j.solmat.2023.112500.

[32] M.K. Hossain, A. Arnab, R.C. Das, K. Hossain, M. Rubel, M.F. Rahman, H. Bencherif, M. Emetere, M.K. Mohammed, R. Pandey, Combined DFT, SCAPS-1D, and wxAMPS frameworks for design optimization of efficient Cs_2BiAgI_6-based perovskite solar cells with different charge transport layers, RSC Adv. 12 (2022) 35002–35025, https://doi.org/10.1039/D2RA06734J.

[33] M.K. Hossain, G.I. Toki, D. Samajdar, M. Mushtaq, M. Rubel, R. Pandey, J. Madan, M.K. Mohammed, M.R. Islam, M.F. Rahman, Deep insights into the coupled optoelectronic and photovoltaic analysis of lead-free $CsSnI_3$ perovskite-based solar cell using DFT calculations and SCAPS-1D simulations, ACS Omega 8 (2023) 22466–22485, https://doi.org/10.1021/acsomega.3c00306.

[34] M.S. Uddin, M.K. Hossain, M.B. Uddin, G.F. Toki, M. Ouladsmane, M.H. Rubel, D.I. Tishkevich, P. Sasikumar, R. Haldhar, R. Pandey, An in-depth investigation of the combined optoelectronic and photovoltaic properties of lead-free $Cs_2AgBiBr_6$ double perovskite solar cells using DFT and SCAPS-1D frameworks, Adv. Electron. Mater. 10 (2024) 2300751, https://doi.org/10.1002/aelm.202300751.

[35] L. Lin, P. Li, L. Jiang, Z. Kang, Q. Yan, H. Xiong, S. Lien, P. Zhang, Y. Qiu, Boosting efficiency up to 25% for HTL-free carbon-based perovskite solar cells by gradient doping using SCAPS simulation, Sol. Energy 215 (2021) 328–334.

[36] A.-A. Kanoun, M.B. Kanoun, A.E. Merad, S. Goumri-Said, Toward development of high-performance perovskite solar cells based on $CH_3NH_3GeI_3$ using computational approach, Sol. Energy 182 (2019) 237–244, https://doi.org/10.1016/j.solener.2019.02.041.

[37] N. Eswaramoorthy, K. Rajaram, 1D graphitic carbon nitride additive modified ZnO electron transport layer for planar perovskite solar cells: 12.22% power conversion efficiency over 1 cm^2 active area, Diam. Relat. Mater. 136 (2023) 109917, https://doi.org/10.1016/j.diamond.2023.109917.

[38] W. Han, F. Fang, Fundamental aspects and recent developments in electropolishing, Int. J. Mach. Tools Manuf. 139 (2019) 1–23, https://doi.org/10.1016/j.ijmachtools.2019.01.001.

[39] S. Rai, B. Pandey, D. Dwivedi, Modeling of highly efficient and low cost $CH_3NH_3Pb(I_{1-x}Cl_x)_3$ based perovskite solar cell by numerical simulation, Opt. Mater. 100 (2020) 109631, https://doi.org/10.1016/j.optmat.2019.109631.

[40] S.T. Jan, M. Noman, Influence of layer thickness, defect density, doping concentration, interface defects, work function, working temperature and reflecting coating on lead-free perovskite solar cell, Sol. Energy 237 (2022) 29–43, https://doi.org/10.1016/j.solener.2022.03.069.

[41] E. Raza, Z. Ahmad, M. Asif, F. Aziz, K. Riaz, M.Q. Mehmood, J. Bhadra, N.J. Al-Thani, Numerical modeling and performance optimization of carbon-based hole transport layer free perovskite solar cells, Opt. Mater. 125 (2022) 112075, https://doi.org/10.1016/j.optmat.2022.112075.

[42] T. Ouslimane, L. Et-Taya, L. Elmaimouni, A. Benami, Impact of absorber layer thickness, defect density, and operating temperature on the performance of $MAPbI_3$ solar cells based on ZnO electron transporting material, Heliyon 7 (2021) e06379, https://doi.org/10.1016/j.heliyon.2021.e06379.

[43] Y. An, A. Shang, G. Cao, S. Wu, D. Ma, X. Li, Perovskite solar cells: optoelectronic simulation and optimization, Sol. RRL 2 (2018) 1800126, https://doi.org/10.1002/solr.201800126.

[44] R. Jeyakumar, A. Bag, R. Nekovei, R. Radhakrishnan, Influence of electron transport layer (TiO_2) thickness and its doping density on the performance of $CH_3NH_3PbI_3$-based planar perovskite solar cells, J. Electron. Mater. 49 (2020) 3533–3539, https://doi.org/10.1007/s11664-020-08041-w.

[45] R. Sharma, A. Sharma, S. Agarwal, M. Dhaka, Stability and efficiency issues, solutions and advancements in perovskite solar cells: a review, Sol. Energy 244 (2022) 516–535, https://doi.org/10.1016/j.solener.2022.08.001.

[46] T. AlZoubi, W.J. Kadhem, M. Al Gharram, G. Makhadmeh, M.A. Abdelfattah, A. Abuelsamen, A.M. AL-Diabat, O. Abu Noqta, B. Lazarevic, S.H. Zyoud, Advanced optoelectronic modeling and optimization of HTL-free $FASnI_3/C_{60}$ perovskite solar cell architecture for superior performance, Nanomaterials 14 (2024) 1062 ⟨https://www.mdpi.com/2079-4991/14/12/1062#⟩.

[47] S. Ghosh, S. Porwal, T. Singh, Investigation of the role of back contact work function for hole transporting layer free perovskite solar cells applications, Optik 256 (2022) 168749, https://doi.org/10.1016/j.ijleo.2022.168749.

[48] M. Omrani, R. Keshavarzi, M. Abdi-Jalebi, P. Gao, Impacts of plasmonic nanoparticles incorporation and interface energy alignment for highly efficient carbon-based perovskite solar cells, Sci. Rep. 12 (2022) 5367, https://doi.org/10.1038/s41598-022-09284-9.

[49] A. Husainat, W. Ali, P. Cofie, J. Attia, J. Fuller, Simulation and analysis of methylammonium lead iodide ($CH_3NH_3PbI_3$) perovskite solar cell with Au contact using SCAPS 1D simulator, Am. J. Opt. Photonics 7 (2019) 33, https://doi.org/10.11648/j.ajop.20190702.12.

[50] N. Rono, A.E. Merad, J.K. Kibet, B.S. Martincigh, V.O. Nyamori, A theoretical investigation of the effect of the hole and electron transport materials on the performance of a lead-free perovskite solar cell based on $CH_3NH_3SnI_3$, J. Comput. Electron. 20 (2021) 993–1005, https://doi.org/10.1007/s10825-021-01673-z.

[51] S. Ijaz, E. Raza, Z. Ahmad, M. Zubair, M.Q. Mehmood, H. Mehmood, Y. Massoud, M.M. Rehman, Numerical simulation to optimize the efficiency of HTM-free perovskite solar cells by ETM engineering, Sol. Energy 250 (2023) 108–118, https://doi.org/10.1016/j.solener.2022.12.027.